ICOMM
2014
No. 30

Design and numerical simulation of an air turbine for a high frequency tool spindle

Christopher Müller[1]; Ingo G. Reichenbach[1]; Jan C. Aurich[1]

[1]*Institute for Manufacturing Technology and Production Systems (FBK), University of Kaiserslautern, Germany*

Abstract

The increasing demand for micro structures and micro parts requires micro tools and precision machines. Furthermore, tool spindles with a very high rotational speed and low run out error are needed to get feasible cutting conditions while machining micro structures and micro parts. The research described in this paper investigates a parameter performance study on an air turbine for a high frequency air bearing spindle, taking into account the inlet nozzle diameter, the air turbine diameter and the gap size between air turbine and housing. The study was performed by computational fluid dynamic (CFD) simulations of the air turbine. The influence of each parameter was analysed and compared to each other. This resulted in a parameter combination that provides the highest power output for the tool spindle.

Keywords: CFD-Simulation, Micromachining, Air turbine, High frequency tool spindle

1. Introduction

The growing demand on micro structures and micro parts requires suitable series production systems and processes with high economic feasibility. Hence, an enormous need for research on the development of cost-efficient manufacturing processes for an inexpensive production of micro structures and parts [1]. A partition of these manufacturing processes is micromachining. To produce forms and structures with micromachining, tools with diameters in the micron range are required. The efficiency of these tools depends on a high rotational speed and a low run out error of the machining spindles [2]. To meet the high demands of rotational speed and run out error, high speed air bearing spindles with rotational speeds above 100,000 rpm are primarily used for micromachining. Spindles are driven by two different concepts, being either driven by electric motors or driven via air turbine, both currently applied. Air turbine driven spindles have the advantage of less installation space, and requires no electric motors, when compared to the electric driven one. The control of the rotational speed and torque is basically a function of the mass flow rate adjusted by a valve. Additionally, the air turbine components are relatively inexpensive to manufacture, so high frequency tool spindles for micromachining, driven by air turbines, have been developed, e.g. by Jahanmir et al., and Waumans et al.. Nevertheless, the air turbines of these spindles have yet not been examined in detail [3,4]. Jackson et al. simulate air turbines for high speed spindles with steady state computational fluid dynamic simulations (CFD) [2]. Thereby, several turbine- and housing geometries were simulated at rotational speeds from 500,000 rpm up to 5,000,000 rpm. The results of these CFD simulations are only available as static pressure coefficients, and cannot determine the torque and power of the air turbines.

Some promising aspects of air turbine design for high speed spindles yield from dental turbine studies, which are used to drive dental drills. These turbines are also driven via compressed air and reach rotational speeds above 300,000 rpm. Moreover, the size of these turbines, from 3.5 - 5 mm, are similar to that of high speed spindles. Experimental studies have been carried out by Dyson et al. regarding reachable torques, drive power and efficiency at different rotational speeds [5,6]. Seto et al. investigated the influence of further design parameters, e.g. nozzle diameter and turbine housing of dental turbine torque and power with an experimental testing system [7]. Chiang et al. used CFD simulations to model the performance of high speed dental air turbines blade rotation [8].

The research presented in this paper shows a Design of Experiments (DoE) based parameter performance study of an air turbine for a high frequency air bearing spindle by means of CFD simulations. It was taken into account the parameters, inlet nozzle diameter, air turbine diameter and the gap size between air turbine and housing. By using DoE, the key design parameters which influence the performance of the air turbine can be further improved.

2. High frequency tool spindle

To achieve a high rotational speed in combination with a low run out error a novel air bearing tool spindle was developed by the Institute for Manufacturing Technology and Production Systems (FBK) [9] (Fig. 1). For that matter, a monolithic rotor tool is guided radially by a journal air bearing and axially by thrust air bearings. Therefore, the air bearings act as a precision interface.

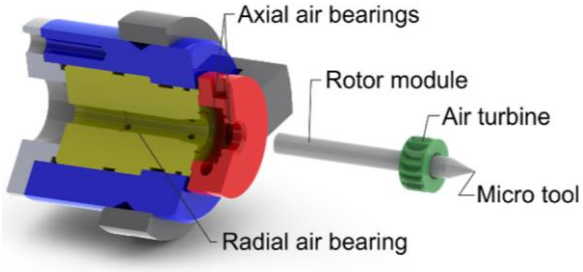

Fig. 1. High frequency tool spindle

The rotor module is driven by an air turbine and it allows a high rotational speed in combination with a run out error < 1 µm. The combination of these properties affords the use of micro end mills and micro grinding tools with a diameter < 100 µm.

Air Turbine Design

The air turbine is shrink fitted on the front end of the rotor module and forms the thrust bearing washers on both sides. With the thrust bearings at the front end, the thermal influence is reduced. While machining with micro tools the air turbine must provide enough power, so calculations with Petroff's equation, which estimates the friction loss in air bearings, show that the air turbine must provide 8.8 W at 300,000 rpm to ensure the processing power for a 100 µm micro end mill [9]. Thereby, over 95 % of the power applied by the turbine is used to compensate the friction loss of the air bearings. To run high rotational speeds in combination with a low run out error, turbine geometry is limited to simple geometries that allow increased balancing quality. Additionally, the turbine must provide enough power at the subsonic inlet mass flow in order to generate less axial vibratory excitation from loading the thrust air bearing with unbalanced forces. CFD simulations were performed by using design of experiments (DoE) to evaluate the influence of the crucial parameters, inlet nozzle diameter, air turbine diameter and gap size between air turbine and housing.

3. Theoretical Model

3.1 Reynolds averaged Navier-Stokes Equations

Continuity equation, momentum equation and energy equation are time averaged to allow numerical computation. These results in the Reynolds-averaged Navier-Stokes Equations are given by [11,12]:

Continuity equation:

$$\frac{\partial \overline{\rho}}{\partial t} + \nabla \cdot \left(\widetilde{\vec{v}} \cdot \overline{\rho} \right) = 0 \tag{1}$$

Momentum Equation:

$$\frac{\partial \left(\overline{\rho} \cdot \widetilde{\vec{v}} \right)}{\partial t} + \overline{\rho} \cdot \left(\widetilde{\vec{v}} \cdot \nabla \right) \cdot \widetilde{\vec{v}} = \widetilde{\vec{k}} - \nabla \overline{p} + \nabla \cdot \overline{\tau} + \nabla \cdot \tau_t \tag{2}$$

Energy Equation:

$$\begin{aligned} &\frac{\partial \left(\overline{\rho} \cdot c_p \cdot \widetilde{T} \right)}{\partial t} + \nabla \left(\overline{\rho} \cdot c_p \cdot \widetilde{T} \cdot \widetilde{\vec{v}} \right) = \\ &\frac{\partial \overline{p}}{\partial t} + \nabla \overline{p} \cdot \widetilde{\vec{v}} + \overline{u'' \cdot \frac{\partial p}{\partial x}} + \overline{v'' \cdot \frac{\partial p}{\partial x}} + \overline{w'' \cdot \frac{\partial p}{\partial x}} + \\ &\frac{\partial}{\partial x} \left(\lambda \cdot \frac{\partial \widetilde{T}}{\partial x} + \lambda \cdot \overline{\frac{\partial T''}{\partial x}} - c_p \cdot \overline{\rho \cdot T'' \cdot u''} \right) + \\ &\frac{\partial}{\partial y} \left(\lambda \cdot \frac{\partial \widetilde{T}}{\partial y} + \lambda \cdot \overline{\frac{\partial T''}{\partial y}} - c_p \cdot \overline{\rho \cdot T'' \cdot v''} \right) + \\ &\frac{\partial}{\partial z} \left(\lambda \cdot \frac{\partial \widetilde{T}}{\partial z} + \lambda \cdot \overline{\frac{\partial T''}{\partial z}} - c_p \cdot \overline{\rho \cdot T'' \cdot w''} \right) + \overline{\rho} \cdot \dot{q}_s + \overline{\psi} \end{aligned} \tag{3}$$

3.2 Finite Volume Method

By using the finite volume method (FVM), values are calculated at discrete places in a meshed geometry (see Fig. 3). Therefore, the conservation laws are applied. The FVM has high accuracy in unstructured meshes. Additionally, it provides results of high accuracy in discontinuous sections, e.g. pressure surges [11].

3.3 Turbulence Model

The flow field in the turbine has Reynolds Numbers between $1 \cdot 10^4$ and $1 \cdot 10^5$, which characterizes a turbulent flow and must be considered within a turbulence model. In this research the shear stress model SST-k-ω, which is a combination of the k-ω and the k-ε model, is used. The k-ω model describes the turbulent kinetic energy (k) and the turbulent frequency (ω) with two partial differential equations. The k-ε model describes the turbulent dissipation (ε) rate and the turbulent kinetic energy (k). The SST-k-ω turbulence model combines the advantages of k-ε model in the core flow with the advantages of the k-ω model at the near-wall regions. Particularly the higher accuracy of the SST-k-ω model at near-wall regions, when compared to other models, is required, since high velocity gradients are expected at the area of the inlet and the turbine. The increased stability of the SST-k-ω model makes another reason for choosing it as the model [13].

3.4 Torque and Power Calculation

The turbine torque is the momentum force which generates the rotation of the rotor module. The torque can be calculated by the turbine blade surface force and the radial position of the blades:

$$T = F \cdot r = \iint p_{abs} \, dA \cdot dr \tag{4}$$

Thereby, F is the blade surface force and r is the radius of the air turbine. The turbine power is calculated by computing the product of torque and rotational speed:

$$P = T \cdot \omega = T \cdot 2\pi \cdot n \tag{5}$$

4. Numerical Simulation

4.1 Geometry and Grid

The computer-aided model (CAD) of the air turbine was used to establish the 3D fluid model, which is simplified into different blocks and meshed with structured and unstructured cells.

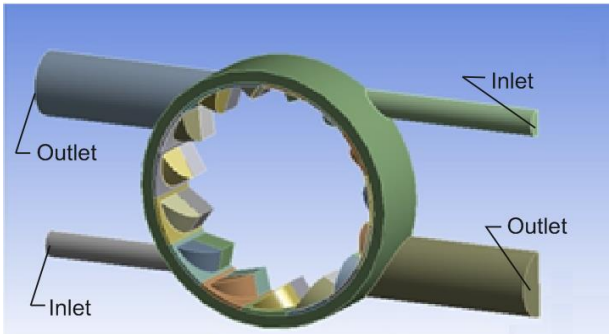

Fig. 2. Air Turbine fluid geometry

Fig. 2 shows one half of the flow geometry with 15 turbine blades and the two inlet nozzles and outlets. Due to the symmetrical structure of the turbine only one half of the model is used for the simulation. As a result simulation times may be reduced.

Fig. 3 shows the mesh of the fluid geometry with unstructured hexahedron cells at the two inlet nozzles, outlets and angularly parts of the turbine blades with inflation layers at the inlet walls.

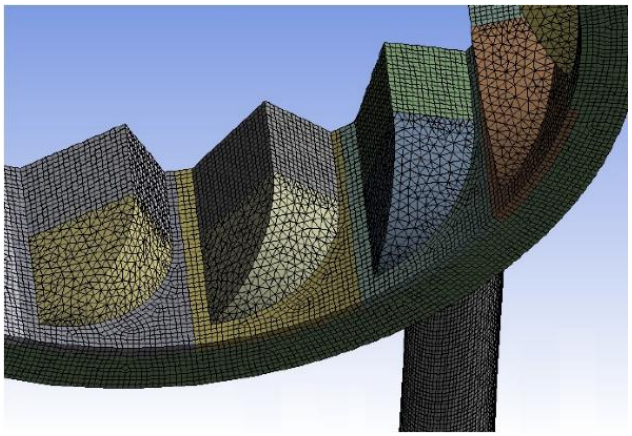

Fig. 3. Mesh of the fluid geometry

The inflation layers are used to get better results at the near wall geometry. The more complex rounded parts of the turbine blades were meshed by an unstructured tetrahedron mesh.

4.2 Moving Reference Frame

In this research the numerical simulations were solved by using the moving reference frame feature in fluent. The moving reference frame method was developed to simulate flows with moving parts, e.g. turbo machinery. Thereby, the transport equations are modified with the inertial forces of the rotation in which the moving reference frame is selected (Fig. 4).

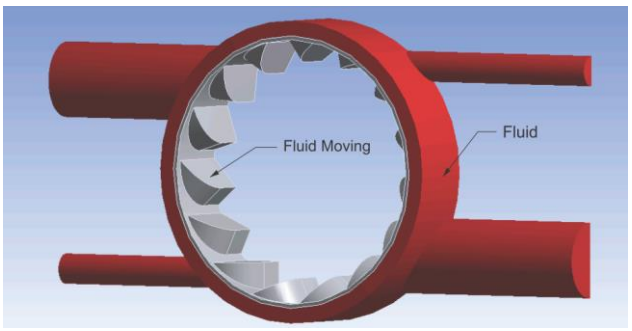

Fig. 4. Fluid geometry with selected moving reference frame

4.3 Numerical Method and Boundary Conditions

The simulations were calculated as transient to get more accurate results. For space discretization the finite volume method with second-order-upwind (2nd Order discretization) principle was used. Therefore an increased simulation stability is able to be achieved in cases of discontinuity. The first order implicit method was used for time discretization. To solve the equations the pressure based SIMPLE-algorithm (Semi-Implicit Method for Pressure-Linked Equations) was applied. The time step size of the transient simulation is set on $\Delta t = 10^{-7}$ s. When the inlet flow is set to subsonic, the Courant number (CFL) can be calculated with the equation (6) [11]:

$$CFL = a\frac{\Delta t}{\Delta x} \tag{6}$$

Considering the sound speed of a = 343.11 m/s at room temperature (20 °C), the smallest mesh size (length of the smallest cell) $\Delta x = 0.01$ mm $= 10^{-5}$ m, and the chosen time step size $\Delta t = 10^{-7}$ s, the calculated Courant number is 3.43. Due to the chosen implicit method for time discretization, the Courant number should be less than 10; this was achieved threefold. To get stationary solutions, 10 turns of the turbine are simulated. With a time step size of $\Delta t = 10^{-7}$ s and 20,000 time steps, an overall simulation time of 0.002 s results from it. Table 1 and Fig. 5 both give an overview of the chosen boundary conditions:

Table 1: Overview of boundary conditions

Boundary	Condition
Inlet 1 and 2	mass flow inlet with subsonic velocity of 330 m/s and 2 bar at 293 K
Outlet 1 and 2	pressure outlet: 1 bar (abs. pressure)
Walls	stationary walls
Symmetry	symmetric wall
Walls Moving	rotating moving wall (300,000 rpm)

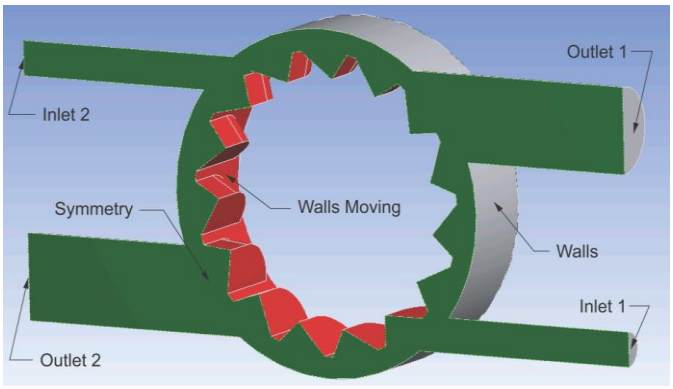

Fig. 5. Fluid geometry with boundary conditions

5. Design of Experiments Parametric Study

Design of Experiments techniques provides a method to determine simultaneously the individual and interactive effects of multiple input variables on an output variable (response). Within the DoE, a central composite experimental design (CCD) was used to minimize the simulation effort and explore the relationship between the parameters:

- Nozzle diameter
- Turbine diameter
- Gap size between turbine blades and housing

In this study, each parameter has five coded levels (-1.682, -1, 0, 1, 1.682) as shown in Table 2. A detailed description of this method is presented by Siebertz et al. and Kleppmann [14,15].

Table 2: Coded and non-coded parameters

Parameter coded	nozzle diameter x_1	turbine diameter x_2	gap size x_3
-1.682	0.4 mm	5.3 mm	0.15 mm
-1	0.6 mm	6 mm	0.3 mm
0	0.8 mm	7 mm	0.5 mm
+1	1.0 mm	8 mm	0.7 mm
+1.682	1.15 mm	9.6 mm	0.85 mm

According to a central composite-second-order rotatable design with 3 independent variables, 15 simulations were conducted with the combination of values shown in Table 3.

Table 3: Experimental design with coded parameters

Configuration No.	Nozzle diameter x_1	Turbine diameter x_2	Gap size x_3
1	-1	-1	-1
2	-1	-1	+1
3	-1	1	-1
4	-1	1	+1
5	+1	-1	-1
6	+1	-1	+1
7	+1	+1	-1
8	+1	+1	+1
9	-1.682	0	0
10	+1.682	0	0
11	0	-1.682	0
12	0	+1.682	0
13	0	0	-1.682
14	0	0	+1.682
15	0	0	0

6. Simulation Results and Discussion

6.1 Velocity and pressure profiles

Fig. 6 shows results for the velocity in configuration 14 and 2

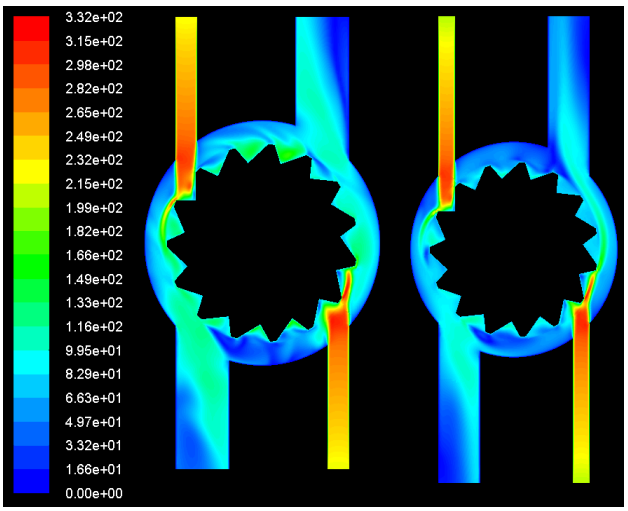

Fig. 6. Calculated velocity in m/s of configuration 14 (left) and 2 (right), after 20,000 time steps (10 revolutions)

The maximal velocity is achieved in the space between the turbine and the inlets due to air expansion. After impact of the inlet flow on the air turbine, the velocity of the gas is insignificantly higher to the turbine rotating speed. Therefore, a large part of the kinetic energy of the flow is transmitted to the turbine by impulse forces.

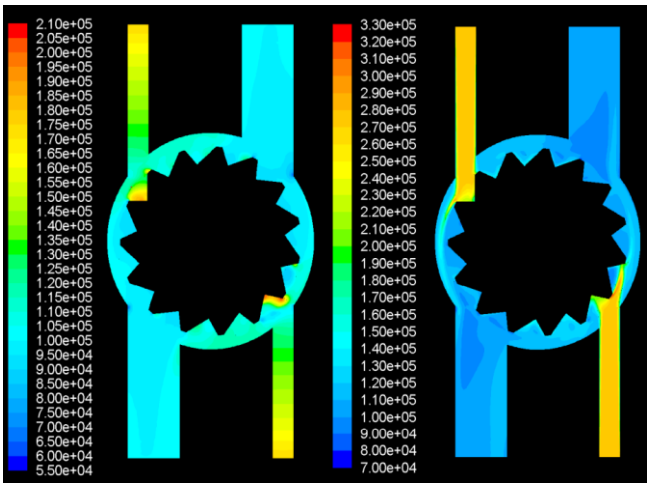

Fig. 7. Calculated static pressure (left) and total pressure (right) in pa of configuration 14, after 20,000 time steps (10 revolutions)

Fig 8 shows the velocity profile of the inlet flow at one turbine blade. It can be seen that the inlet flow is deflected almost 180 degrees. This is an indication for good impulse transmission.

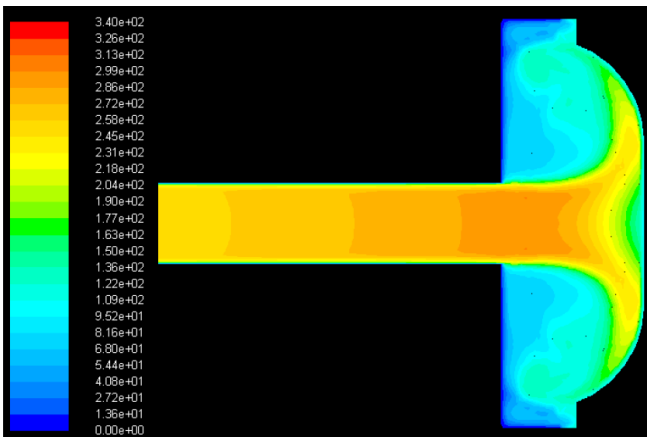

Fig. 8. Velocity profile in m/s of the inlet flow at the turbine blade

6.2 Evaluation of DoE

Fig. 9 shows the simulated results for the 15 different configurations (see Table 3). The configuration no. 8 (+1 +1 +1) gives out the best performance (10.9 W). The worst configuration is no. 9 (-1.682 0 0) with a power of 2.1 W.

With the results of the 15 simulations, a quadratic regression with single interactions was performed according to the equation (7) [7].

$$\hat{y} = \beta_0 + \beta_1 \cdot x_1 + \beta_2 \cdot x_2 + \beta_3 \cdot x_3 + \beta_4 \cdot x_1 \cdot x_2 + \beta_5 \cdot x_1 \cdot x_3 + \beta_6 \cdot x_2 \cdot x_3 + \beta_7 \cdot x_1^2 + \beta_8 \cdot x_2^2 + \beta_9 \cdot x_3^2 = \hat{y} = X \cdot \beta \quad (7)$$

Thereby, X is the design matrix, and β_n are the regression coefficients. To obtain regression coefficients, equation (8) can be solved by:

$$\beta = X^{-1} \cdot y = (X^T \cdot X)^{-1} \cdot X^T \cdot y \quad (8)$$

The values in table 4 are the regression coefficients calculated according to equation (8):

Table 4: Regression coefficients

No.	Design parameter	β_n in W
0	-	7.257
1	x_1	2.376
2	x_2	-0.118
3	x_3	0.141
4	$x_1 \cdot x_2$	0.118
5	$x_1 \cdot x_3$	0.406
6	$x_2 \cdot x_3$	0.218
7	x_1^2	-0.404
8	x_2^2	-0.384
9	x_3^3	0.065

Fig. 9 shows an overview of the simulated results and the design points given by the regression. Only a small deviation of the design points to the simulated results can be seen. Consequently, there is a good adaption of the design points to the simulated results.

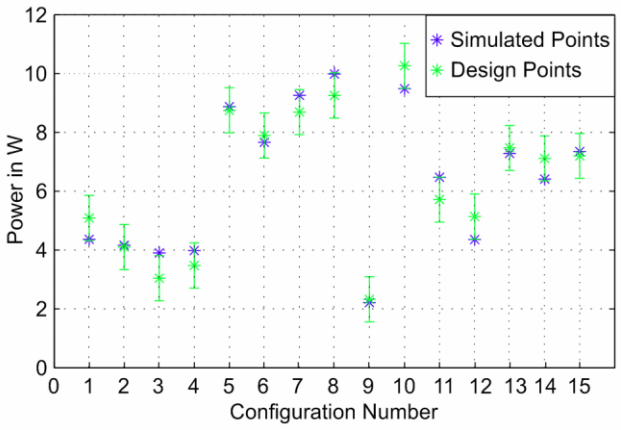

Fig. 9. Simulation results and design points of regression for different configurations

6.3 Response surface plots

Fig. 10, 11 and 12 show the response surface plots of the two different variables by a constant third variable. On Fig. 10 it can be seen that the nozzle diameter (x_1) has the highest influence on the power of the air turbine. By increasing nozzle diameter, the mass flow rate increases as does the energy given to the air turbine blades.

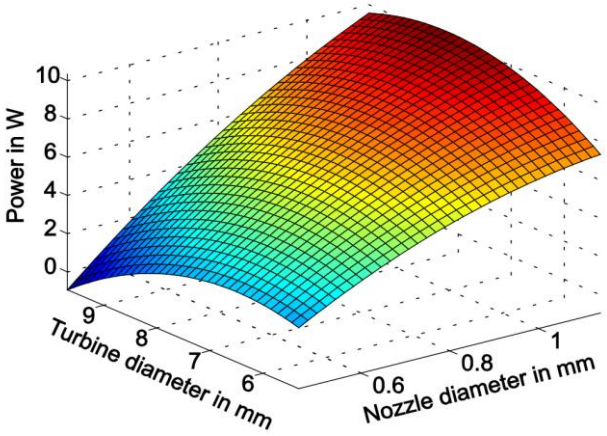

Fig. 10. Effect of turbine- and nozzle diameter on air turbine power at constant gap size (0.5 mm)

A turbine diameter (x_2) of 7.5 mm ensures the maximum power. This maximum is a result of the inflow velocity, which is confined to the subsonic flow. By increasing the diameter of the turbine, the circumferential velocity increases. Thereby, the subsonic flow cannot generate enough pressure on the turbine blades.

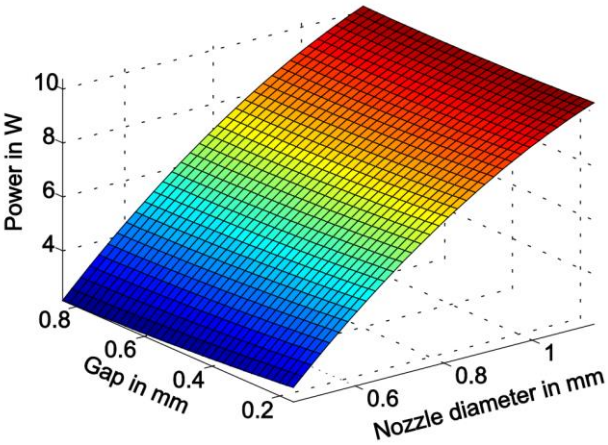

Fig. 11. Effect of gap size and nozzle diameter on air turbine power at constant turbine diameter (7 mm)

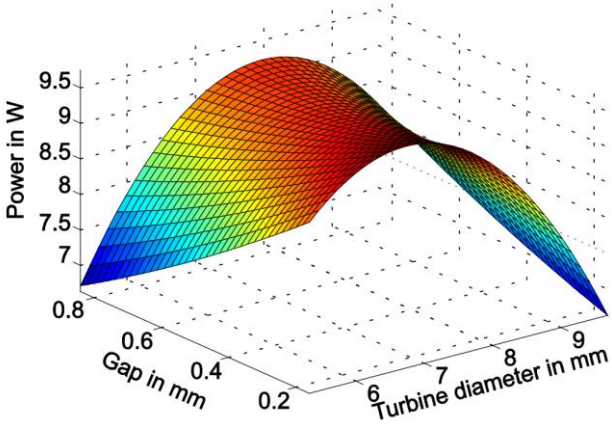

Fig. 12. Effect of gap size and turbine diameter on air turbine at constant nozzle diameter (0.5 mm)

Reducing the gap between air turbine and housing increases the power of the air turbine, because at the same time the fraction of flow passing through the turbine blades without interaction decreases (Fig. 12). The resulted regression function can be used to find a design configuration with maximum drive capacity. This configuration has the following code values of x_1=1.682, x_2=0.7, x_3=-1.6, and a drive capacity of about 12 W.

7. Conclusions and Outlook

The research described in this paper investigates the impact of geometrical air turbine parameters on the power output of a high frequency tool spindle. Therefore, the geometrical parameters, inlet nozzle diameter, air turbine diameter and gap size between air turbine and housing was varied. The results show that all of the investigated parameters contribute to the performance of the air turbine. The optimal parameters within this study are 1.15 mm for the nozzle diameter, 7.3 mm for the air turbine diameter and 0.1 mm for the gap between turbine and housing. The simulation results will be verified by a high frequency tool spindle with the best air turbine parameter combination. To capture data such as power output, run out error and rotational frequency, a test rig will assembled to test the new air turbine drive geometry in the existing spindle.

Nomenclature

CFL	courant no.	-
c_p	heat capacity at constant volume	in J/kg/K
k	Specific turbulent kinetic engergy	in m²/s²
n	rotational speed	1/s
P	power	in W
p_{kin}	kinetic pressure	in Pa
p_{stat}	static pressure	in Pa
q_s	heat flow	in kg m²/s³
T	temperature	in K
t	time	in s
u,v,w	velocity	in m/s
x,y,z	cartesian coordinates	-
τ	friction tensor	in N/m²
τ_t	turbulent friction tensor	in N/m²
λ	heat conductivity	W/m K
ρ	density	kg/m³
∇	nablaoperator	-

Acknowledgement

The research described in this paper was supported by the German Research Foundation (DFG) within the Priority Program SPP 1476 AU 185/24-1: ‘‘Small machine tools for small workpieces’’.

References

[1] Dornfeld, D.; Min, S.; Takeuchi; Y: Recent Advances in Mechanical Micromachining. CIRP Annals, 55 (2006) 2: pp. 745-768.

[2] Jackson, M.J.; Robinson, G.M; Hyde, L.J; Kanjarkar, K.; Cui, J.: Design and manufacture of high-speed spindles for dry micromachining applications. International Journal of Nanofactoring 1 (2007) 5: pp. 641–656.

[3] Jahanmir, S.; Ren, Z.; Heshmat, H.; Tomaszewski, M.: Design and evaluation of an ultrahigh speed micro-machining spindle. Machining Science and Technology 14 (2010) 2: pp. 224-243.

[4] Waumans, T.; Vleugels, P; Peirs, J; Al-Bender, F; Reynaerts, D: Rotordynamic behaviour of a micro turbine rotor on air bearings. Proceedings of the International Conference on Noise and Vibration Engineering. 18-20 September 2006, Leuven, Belgium: pp. 181-197.

[5] Dyson, J.E.; Darvell, B.W.: Flow and free running speed characterization of dental air turbine handpieces; Journal of Dentistry 27 (1999), pp. 465-477.

[6] Dyson, J.E.; Darvell, B.W.: Torque, power and efficiency characterization of dental air turbine handpieces; Journal of Dentistry, 27 (1999). pp. 573-586.

[7] Seto, A.: Design Factors Affecting Air Turbine Handpiece Performance; Dissertation, University of Hong Kong (2005).

[8] Chiang, H.W. D.; Hsu, C.N.; Chang, Y.Y.: Numerical Simulation and Experimental Study of a Dental Handpiece Air Turbine; Int. J. Turbo Jet-Engines, 28 (2011). pp. 159-168.

[9] Aurich, J.C.; Müller, C.; Walk, M.: High-frequency tool-spindle for multifunctional, replaceable rotor-modules. Production Engineering 7 (2013) 5: pp. 555-560.

[10] Bartz, W.J: Luftlagerungen. Grundlagen und Anwendungen. Expert-Verlag Ehningen (1993).

[11] Oertel, H.; Böhle, M.; Dohrmann, U.: Strömungsmechanik. Vieweg-Teubner Wiesbaden (2009).

[12] Went, J.: Computational Fluid Dynamics. Springer Berlin, Heidelberg (2008).

[13] Chung, T.J.: Computational Fluid Dynamics. Cambridge University Press Cambridge (2010).

[14] Siebertz, K.; Bebber, D.; Hochkirchen, T.: Design of Experiments (DoE). Springer Heidelberg (2010).

[15] Kleppmann, W.: Taschenbuch Versuchsplanung Hanser München (2008).